

Protective effects of zingerone against sodium arsenite-induced lung toxicity: A multi-biomarker approach

Hasan Şimşek^{1*}, Sefa Küçükler², Cihan Gür², Mustafa İleritürk³, Serpil Aygörmüş⁴, Fatih Mehmet Kandemir⁵

¹ Department of Physiology, Faculty of Medicine, Aksaray University, Aksaray, Türkiye

² Department of Veterinary Biochemistry, Faculty of Veterinary, Atatürk University, Erzurum, Türkiye

³ Department of Animal Science, Horasan Vocational College, Atatürk University, Erzurum, Türkiye

⁴ Department of Veterinary Biochemistry, Faculty of Veterinary, Kafkas University, Kars, Türkiye

⁵ Department of Medical Biochemistry, Faculty of Medicine, Aksaray University, Aksaray, Türkiye

ARTICLE INFO

Article type:

Original

Article history:

Received: Apr 20, 2023

Accepted: Jul 2, 2023

Keywords:

Apoptosis
Autophagy
Inflammation
Lung
Oxidative stress
Sodium arsenite
Toxicity
Zingerone

ABSTRACT

Objective(s): Sodium arsenite (SA) exposure is toxic to the body. Zingerone (ZNG) is a flavonoid with many biological properties found naturally in honey and plants. This study aimed to determine the effects of ZNG on SA-induced rat lung toxicity.

Materials and Methods: Thirty-five male Sprague rats were divided into Control, SA, ZNG, SA+ZNG25, and SA+ZNG50 groups (n=7). SA 10 mg/kg and ZNG were administered at two doses (25 and 50 mg/kg) (orally, 14 days). Analysis of oxidative stress, inflammation damage, apoptosis damage, and autophagic damage markers in lung tissue were determined by biochemical and histological methods.

Results: The administration of ZNG reduced oxidative stress by increasing SA-induced decreased antioxidant enzyme activities, increasing Nrf-2, HO-1, and NQO1, and decreasing MDA level. ZNG administration reduced inflammation marker levels. Anti-apoptotic Bcl-2 increased and apoptotic Bax and Caspase-3 decreased with ZNG. ZNG promoted the regression of autophagy by reducing Beclin-1, LC3A, and LC3B levels.

Conclusion: Evaluating all data showed that SA caused toxic damage to lung tissue by increasing inflammation, apoptosis, autophagy, and oxidant levels, whereas ZNG had a protective effect by reducing this damage.

► Please cite this article as:

Şimşek H, Küçükler S, Gür C, İleritürk M, Aygörmüş S, Kandemir FM. Protective effects of zingerone against sodium arsenite-induced lung toxicity: A multi-biomarker approach. Iran J Basic Med Sci 2023; 26: 1098-1106. doi: <https://dx.doi.org/10.22038/IJBMS.2023.71905.15623>

Introduction

Heavy metals have become a major concern for human health and environmental toxicology as a result of advances in agriculture and industry, owing to their increasing bioaccumulation, toxicity, and persistence in aquatic ecosystems (1). Arsenic (AR), which ranks 20th in terms of its presence in soil, is one of the toxic heavy metals with the highest environmental or occupational exposure (2, 3). Long-term exposure to AR, particularly from drinking water, is a public health hazard. Studies have reported that around 200 million people are chronically exposed to toxic levels of AR (4). Even at low concentrations, AR causes toxicity (5). AR exposure is known to induce reactive oxygen species (ROS) generation resulting in lipid peroxidation (LP), protein oxidation, and DNA damage, the mechanisms underlying AR toxicity have not yet been fully elucidated (6).

Moreover, AR compounds are also dangerous and are among the toxic substances known to be carcinogenic to humans. Sodium arsenite (SA) is the most dangerous among these compounds to human and animal health (7). AR compounds are used in the production of specialty glass, wood preservatives, herbicides, insecticides, and drugs used to treat blood cancer (8). Arsenite, a toxic inorganic trivalent arsenic compound (As³⁺) with potent toxicity, has a direct affinity for the sulfhydryl group and causes a

significant increase of ROS in many tissues (9). Exposure to toxic substances such as As³⁺ induces oxidative stress (OS) damage due to increased ROS and therefore anti-oxidants may be required to maintain oxidant/anti-oxidant homeostasis (5). Recent research has determined that natural plant-derived substances are effective in reducing AR toxicity in various organs and tissues (6).

Flavonoids are plant anti-oxidants that show biological and pharmacological properties in many cell types *in vivo* and *in vitro* (10). One of these flavonoids, zingerone (ZNG), is released in the dried form of ginger and during the contact of gingerols with heat, and its most remarkable feature is that it is a powerful anti-oxidant (11). Aside from its anti-oxidant properties, ZNG also affects signaling pathways involved in many cellular metabolic pathways. Previous research has reported that ZNG has many important biological activities, especially anti-oxidant properties (12). ZNG presents these effects by reducing ROS production, suppressing inflammatory cytokine transcription, inhibiting Nuclear factor kappa-B (NF-κB), inhibiting apoptotic pathways, and up-regulating anti-oxidants (13).

Studies to minimize heavy metal-induced toxicity damage, which has increased due to increased environmental pollution, have recently come to the fore. In this context, this study aimed to determine the curative effects of ZNG,

*Corresponding author: Hasan Şimşek. Department of Physiology, Faculty of Medicine, Aksaray University, Aksaray, Türkiye. Email: hasansimsek47@gmail.com

a plant-derived substance, on SA-induced lung toxicity. For this purpose, the effects of ZNG on OS damage caused by SA in lung tissue and inflammation, apoptotic, autophagy, and LP damages triggered by this damage were determined by biochemical, molecular, and histological methods.

Materials and Methods

Chemicals

SA, ZNG, and all other chemicals were obtained from Sigma (MO, USA). All chemicals were of analytical purity.

Animals and experimental protocol

Thirty-five Sprague Dawley rats (220–250 g, male, 12–14 weeks) were employed in the experiments. Rats were obtained from Atatürk University Laboratory Animal Centre (Erzurum, Turkey). Rats were housed under ventilated standard conditions of 12 hr of light/dark, $45 \pm 5\%$ humidity, and $23 \pm 2^\circ\text{C}$. Rats had free access to feed and water. They were randomly divided into five groups ($n=7$). SA and ZNG doses were determined from the literature (5, 12, 14).

Control: Saline was given orally once a day for 14 days.

Sodium Arsenite (SA): SA was given orally at a dose of 10 mg/kg for 14 days.

Zingerone (ZNG 50 mg/kg): 50 mg/kg dose was given orally for 14 days.

Sodium Arsenite + Zingerone 25 mg/kg (SA+ZNG25 mg/kg): SA was given at a dose of 10 mg/kg followed by ZNG 25 mg/kg orally for 14 days.

Sodium Arsenite + Zingerone 50 mg/kg (SA+ZNG50 mg/kg): SA was given at a dose of 10 mg/kg followed by ZNG 50 mg/kg orally for 14 days.

Collection of samples

Rats were decapitated under anesthesia (mild sevoflurane) 24 hr after the last ZNG administration (day 15). Lung tissues were then collected. They tissues were separated from the surrounding tissues, washed with cold saline, and divided into two parts. One part was stored at -80°C for biochemical and molecular analysis. The other part was placed in a 10% formaldehyde solution for histopathologic examination.

Analysis of lipid peroxidation

LP levels of lung tissues were determined with malondialdehyde (MDA) level. To determine the level of MDA, it was reacted with thiobarbituric acid, and the color formed was measured by absorbance at the 532-nanometer wavelength. Lung tissues were homogenized with 1.15% potassium chloride using a Tissue Lyser II homogenizer (Qiagen, The Netherlands). The homogenates obtained were centrifuged at 4°C and 1,000xg for 15 min, and the supernatant was collected and used in the analysis. MDA levels were determined according to the previous study (15).

Anti-oxidant analysis

Catalase (CAT), superoxide dismutase (SOD), glutathione peroxidase (GPx) activities, and glutathione (GSH) levels were measured for the anti-oxidant status of lung tissues. The supernatants used for the analysis of CAT, SOD, GPx, and GSH were obtained in a similar manner as in LP. CAT, SOD, GPx, and GSH were determined according to the methods of Aebi (16), Sun *et al.* (17), Lawrence and Burk (18), and Sedlak and Lindsay (19), respectively. The total protein content of tissues, which is necessary for the

calculation of enzyme activities, was determined by the method of Lowry *et al.* (20).

Analysis of mRNA transcript levels by real-time PCR (RT-PCR)

The RT-PCR method was used to determine the mRNA transcript levels of significant genes involved in OS damage, inflammation damage, apoptotic damage, and autophagic damage. Total RNA isolation from rat lung tissues was performed using QIAzol Lysis Reagent (79306; Qiagen) and RNA content was measured with NanoDrop (BioTek Epoch) device. RNAs were then converted into cDNAs using iScript cDNA Synthesis Kit (Bio-Rad), and cDNA concentrations were measured with NanoDrop (BioTek Epoch). The relative mRNA transcript levels of the primer sequences shown in Table 1 were determined by Rotor-Gene Q (Qiagen) using iTaq Universal SYBR Green Supermix (BIO-RAD) according to the manufacturer's instructions. The CT values obtained were normalized according to β -Actin using the $2^{-\Delta\Delta\text{CT}}$ method (21).

Western blot analysis

Western blot analysis of lung tissues was accomplished using the method of Ileriturk *et al.* (22). Lung tissues pulverized with liquid nitrogen were weighed and homogenized in RIPA buffer. Once homogenized, they were centrifuged (16,000g, 20 min). The total protein in the

Table 1. The primer sequences of the related genes used in the RT-PCR (R: Reverse; F: Forward)

Gene	Sequences (5'-3')	Length (bp)	Accession no.
Nrf2	F: TTTGTAGATGACCATGAGTCGC R: TCCTGCGCAAACCTGTCCAT	161	NM_031789.2
HO-1	F: ATGTCCCAGGATTTGTCCGA R: ATGGTACAAGGAGGCCATCA	144	NM_012580.2
NQO1	F: CTGGCCAATTCAGAGTGGCA R: GATCTGGTTGTCGGCTGGAA	304	NM_017000.3
NF- κ B	F: AGTCCCGCCCTTCTAAAAC R: CAATGGCCTCTGTGTAGCCC	106	NM_001276711.1
TNF- α	F: CTCGAGTGACAAGCCCGTAG R: ATCTGCTGGTACCACAGTT	139	NM_012675.3
IL-1 β	F: ATGGCAACTGTCCCTGAACT R: AGTGACACTGCCTTCTGAA	197	NM_031512.2
COX-2	F: AGGTTCTTCTGAGGAGAGAG R: CTCACCAGTACCTGATAT	240	NM_017232.3
iNOS	F: AGATCAATGCAGCTGTGCTC R: GGCTCGATCTGGTAGTAGATA	235	NM_012611.3
IL-6	F: AGCGATGATGCACTGTCAGA R: GGAACCTCAGAAGACCAGAGC	127	NM_012589.2
MAPK14	F: GTGGCAGTGAAGAAGCTGTC R: GTCACCAGGTACACATCGTT	170	NM_031020.2
Bax	F: TTTTCATCCAGGATCGAGCAG R: AATCATCTCTGCAGCTCCA	154	NM_017059.2
Bcl-2	F: GACTTTGAGAGATGTCAG R: TCAGGTAICTCAGTCATCCAC	214	NM_016993.2
Caspase-3	F: ACTGGAATGTCAGCTCGCAA R: GCAGTAGTCGCCTCTGAAGA	270	NM_012922.2
Beclin-1	F: TCTCGTCAAGCGTCACTTC R: CCATTCTTTAGGCCCGACG	198	NM_053739.2
LC3A	F: GACCATGTTAACATGAGCGA R: CCTGTTCATAGATGTCAGCG	139	NM_199500.2
LC3B	F: GAGCTTCGAACAAGAGTGG R: CGCTCATATTCACGTGATCA	152	NM_022867.2
β -Actin	F: CAGCCTTCCTCTGGGTATG R: AGCTCAGTAAACAGTCCGCCT	360	NM_031144.3

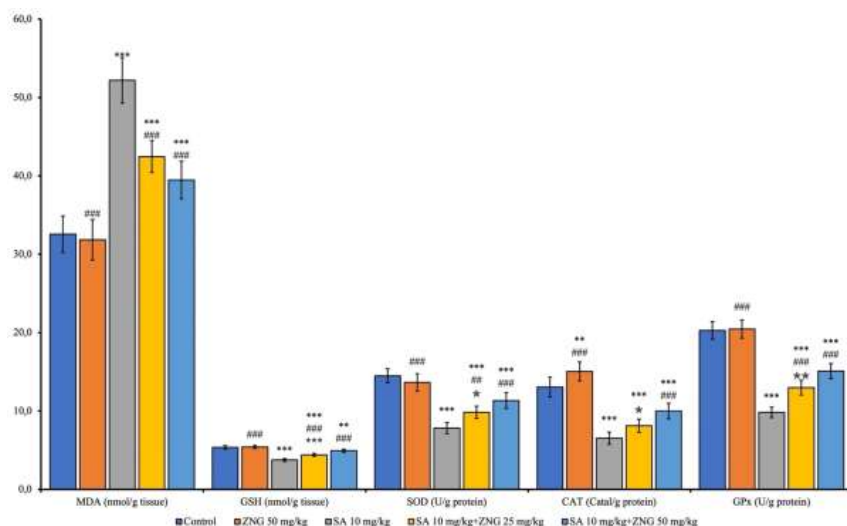


Figure 1. Lipid peroxidation and anti-oxidant levels in rat lung tissue

MDA: Malondialdehyde, GSH: Glutathione, SOD: Superoxide dismutase, CAT: Catalase, GPx: Glutathione peroxidase

Statistical significance was analyzed using One Way ANOVA (mean \pm SD) (Control vs others: * P <0.05, ** P <0.01, *** P <0.001, SA 10 mg/kg vs others: # P <0.05, ## P <0.01, ### P <0.001, SA 10 mg/kg+ZNG 25 mg/kg vs SA 10 mg/kg+ZNG 50 mg/kg: ☆ P <0.05, ☆☆ P <0.01, ☆☆☆ P <0.001).

supernatants was determined using the Thermo Fischer™ protein BCA assay kit. After protein measurement, supernatants were diluted with Laemmli sample buffer. The supernatants were separated by 10% sodium dodecyl sulfate-polyacrylamide gel electrophoresis with 30 μ g protein in each well. Proteins separated by molecular size were transferred into PVDF membranes. After the proteins were transferred to the membranes, they were blocked with 4% Bovine serum albumin dissolved in phosphate-buffered saline with 0.1% tween (PBS-T) for 1.5 hr. Following this, proteins were incubated overnight together with the primary antibodies. At the end of incubation, goat anti-mouse IgG secondary antibody conjugated to HRP was incubated for 1.5 hr (1:2,000 dilution). After incubation with secondary antibodies, the membranes were washed five times with PBS-T for five min each time. The bands were then visualized with BioRad Clarity Max ECL substrate (Bio-Rad, Hercules, USA). Blots were subjected to densitometric analysis with the ImageLab program (Bio-Rad, Hercules, USA). At least three replicate measurements were taken.

Histopathological evaluations

Lung tissues were kept in a 10% neutral formalin buffer for 24 hr. After tissue follow-up, five μ m thick sections were taken from the paraffin blocks with a microtome. The sections were placed on slides and stained with hematoxylin and eosin (H&E) stains. The stained samples were examined and photographed with an Olympus Cx 43 microscope (Japan).

Statistical analysis

Statistical analysis of the data obtained from lung tissues was performed with SPSS 20.0 (IBM, NY, USA) program. One-way ANOVA and Tukey's *post hoc* tests were used for comparison between groups. In the RT-PCR method, each sample was run in triplicate. Data are presented as mean \pm SD. Statistical significance was accepted at three levels: P <0.05, P <0.01, and P <0.001.

Results

Effects of SA and ZNG administrations on oxidative stress

MDA levels, an indicator of LP, increased (P <0.001);

and analyzed anti-oxidants decreased (P <0.001) with SA administration. Compared to the SA group, SOD (P <0.01), GPx, and GSH increased (P <0.001); MDA decreased (P <0.001) in the SA+ZNG 25mg/kg group. These effects were more in the SA+ZNG50mg/kg group (P <0.001 in all parameters) (Figure 1).

Effects of SA and ZNG administrations on Nrf-2, HO-1, and NQO1 mRNA transcription

Compared to the control, Nuclear factor erythroid 2-related factor 2 (Nrf-2), Heme Oxygenase 1 (HO-1), and NAD(P) H Quinone Dehydrogenase 1 (NQO1) levels decreased in the SA group (P <0.001). Compared to the SA group, these parameters were increased in the SA+ZNG25mg/kg and SA+ZNG50mg/kg groups (P <0.001). In 50 mg/kg dose compared to 25 mg/kg dose, this increase was even more significant in the HO-1 parameter (P <0.01) (Figure 2).

Effects of SA and ZNG administrations on inflammation marker mRNA transcription

NF- κ B, Tumor Necrosis Factor- α (TNF- α), Interleukin-1

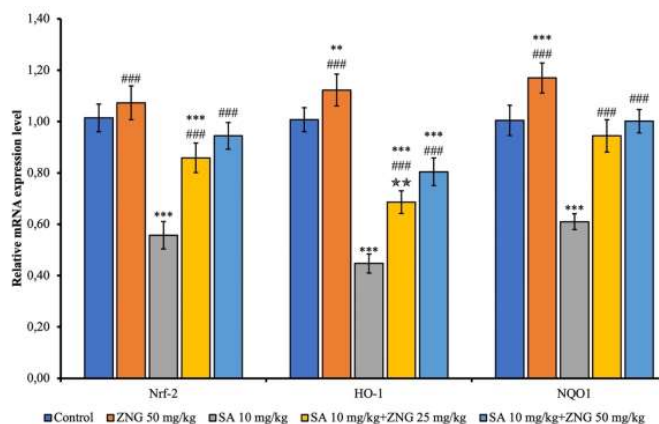


Figure 2. Nrf-2, HO-1, and NQO1 mRNA transcript levels in rat lung tissue Nrf-2: Nuclear factor erythroid 2-related factor 2, HO-1: Heme oxygenase 1, NQO1: NAD(P)H Quinone Dehydrogenase 1. Statistical significance was analyzed using One Way ANOVA (mean \pm SD) (Control vs others: * P <0.05, ** P <0.01, *** P <0.001, SA10 mg/kg vs others: # P <0.05, ## P <0.01, ### P <0.001, SA 10 mg/kg+ZNG 25 mg/kg vs SA 10 mg/kg+ZNG 50 mg/kg: ☆ P <0.05, ☆☆ P <0.01, ☆☆☆ P <0.001)

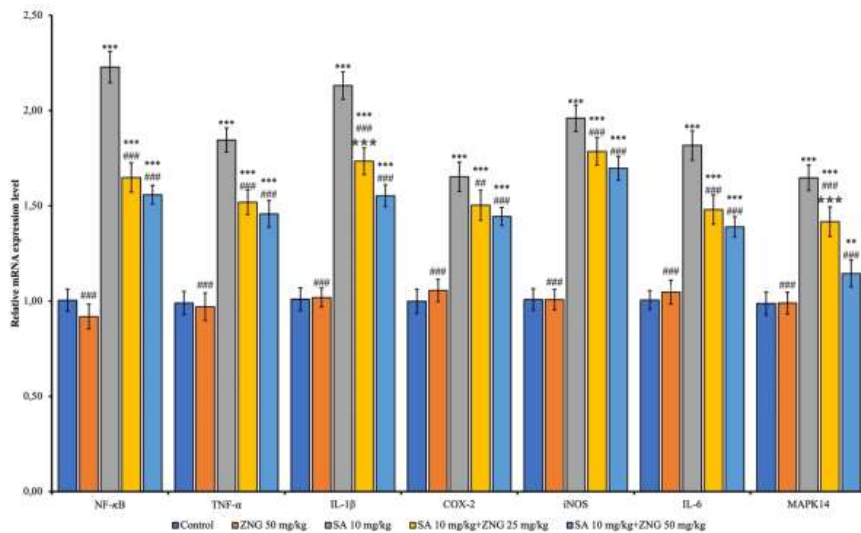


Figure 3. mRNA transcript levels of inflammation markers in the rat lung tissues

NF- κ B: Nuclear factor kappa-B, TNF- α : tumor necrosis factor-alpha, IL-1 β : interleukin-1 beta, COX-2: cyclooxygenase-2, iNOS: inducible nitric oxide synthase, IL-6: Interleukin-6. Statistical significance was analyzed using One Way ANOVA (mean \pm SD) (Control vs others: * P <0.05, ** P <0.01, *** P <0.001, SA 10 mg/kg vs others: # P <0.05, ## P <0.01, ### P <0.001, SA 10 mg/kg+ZNG 25 mg/kg vs SA 10 mg/kg+ZNG 50 mg/kg: ☆ P <0.05, ☆☆ P <0.01, ☆☆☆ P <0.001)

beta (IL-1 β), Cyclooxygenase-2 (COX-2), Inducible nitric oxide synthase (iNOS), Interleukin-6 (IL-6), and Mitogen-Activated Protein Kinase 14 (MAPK14) mRNA transcript levels were determined by RT-PCR method. Compared to the control, mRNA transcript levels of all these parameters increased in the SA group (P <0.001). COX-2 (P <0.01) and all other parameters (P <0.001) decreased in the SA+ZNG25mg/kg group compared to the SA group. Transcript levels of all these parameters decreased in SA+ZNG50mg/kg group compared to the SA group (P <0.001) (Figure 3).

Effects of SA and ZNG administrations on apoptotic markers

Apoptotic factors (Bax and Caspase-3) increased (P <0.001) and antiapoptotic factor B-cell lymphoma 2 (Bcl-2) decreased (P <0.001) with SA administration. SA+ZNG25mg/kg and

SA+ZNG50mg/kg groups had decreased apoptotic factors and increased antiapoptotic factors compared to the SA group (P <0.001). The increase in Bcl-2 (P <0.001) and decrease in Bax (P <0.05) and Caspase-3 (P <0.001) were more pronounced at the higher dose (Figure 4).

Effects of SA and ZNG administrations on autophagy markers

Beclin-1, Microtubule-associated protein 1 light chain 3 alpha (LC3A) and Microtubule-associated protein 1 light chain 3 beta (LC3B) mRNA transcript levels were measured to analyze the autophagy level in lung tissues. The mRNA transcription levels of Beclin-1, LC3A, and LC3B were increased by SA treatment (P <0.001). Transcript levels of these parameters decreased in SA+ZNG25mg/kg and SA+ZNG50 mg/kg groups compared to the SA group

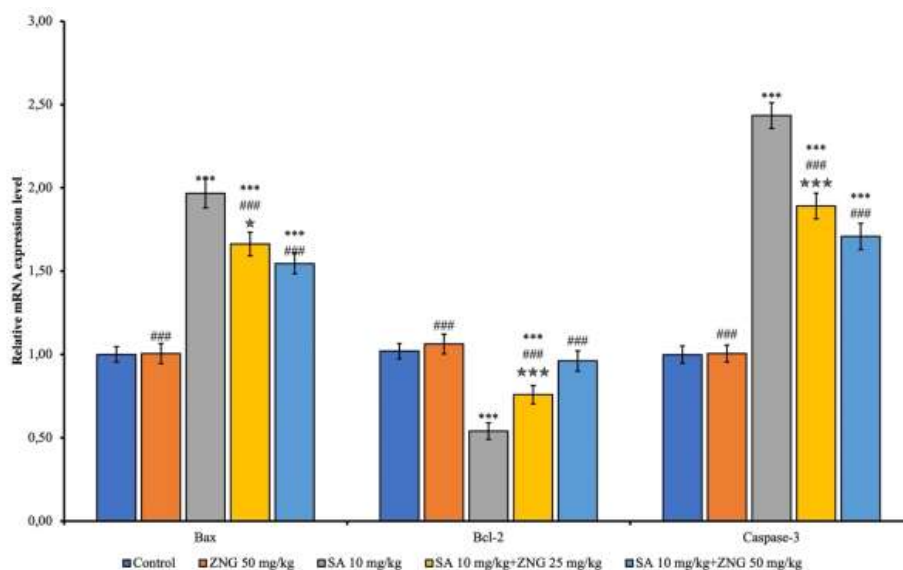


Figure 4. mRNA transcript level of apoptotic markers in the rat lung tissues

Bcl-2: B-cell lymphoma 2, Caspase-3: cysteine-aspartic acid protease. Statistical significance was analyzed using One Way ANOVA (mean \pm SD) (Control vs others: * P <0.05, ** P <0.01, *** P <0.001, SA10mg/kg vs others: # P <0.05, ## P <0.01, ### P <0.001, SA10mg/kg+ZNG25 mg/kg vs SA10 mg/kg+ZNG50 mg/kg: ☆ P <0.05, ☆☆ P <0.01, ☆☆☆ P <0.001).

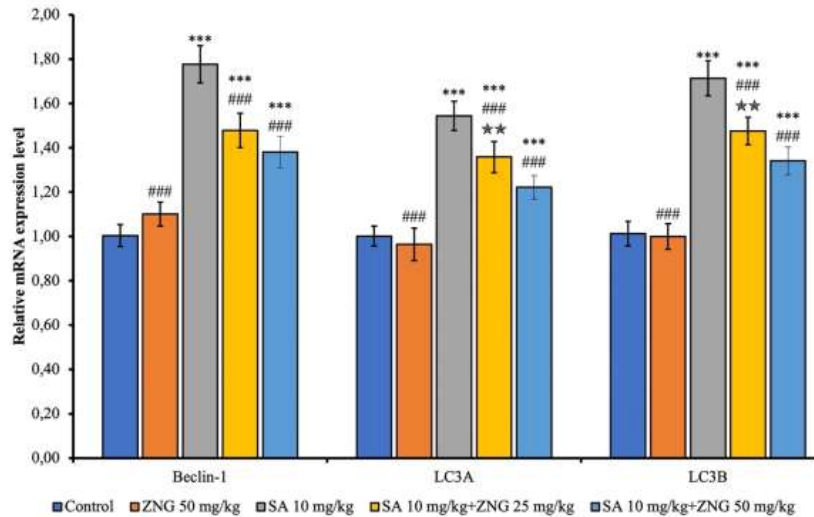


Figure 5. mRNA transcript levels of autophagy markers in the rat lung tissues
 LC3A: Microtubule-associated protein 1 light chain 3 alpha, LC3B: Microtubule-associated protein 1 light chain 3 beta. Statistical significance was analyzed using One Way ANOVA (mean ± SD) (Control vs others: *P<0.05, **P<0.01, ***P<0.001, SA 10 mg/kg vs others: #P<0.05, ##P<0.01, ###P<0.001, SA 10 mg/kg+ZNG25 mg/kg vs SA 10 mg/kg+ZNG 50 mg/kg: ☆P<0.05, ☆☆P<0.01, ☆☆☆P<0.001).

(P<0.001). When the doses were compared, the decrease in LC3A and LC3B parameters was higher at 50 mg/kg dose (P<0.01) (Figure 5).

Effects of SA and ZNG administrations on IL-1β, NF-κB, and Beclin-1 protein levels

IL-1β, NF-κB, and Beclin-1 protein levels were increased with SA treatment (P<0.001) Compared to the SA group, it was found that IL-1β and Beclin-1 levels decreased in the SA+ZNG25mg/kg group (P<0.05), while IL-1β (P<0.001), NF-κB (P<0.01), and Beclin-1 (P<0.001) decreased in the SA+ZNG50mg/kg group (Figure 6).

Histopathological findings

Figure 7 shows the effects of ZNG on SA-induced histological changes in lung tissues using H&E staining.

The lung tissues of both the control and ZNG groups had healthy histologic structures and no significant damage. In particular, alveolar septal thickness was normal, and bronchial and bronchial epithelial cells were arranged well (Figure 7A, 7B). When the sections in the SA group were examined, alveolar septal thickening and inflammatory cell infiltration were observed especially in the lung tissue. Hemorrhages and congestion in the interstitial space were particularly noticeable in this group. Some images showed alveolar enlargement, vacuoles, and edema. In conclusion, SA administration was found to impair lung morphology (Figure 7C). It was observed that the administration of ZNG in combination with SA reduced inflammatory cell infiltration and relieved hemorrhages in a dose-dependent manner. In this group, lung wall thickening was observed at a minimal level, especially at high doses (Figure 7D, 7E).

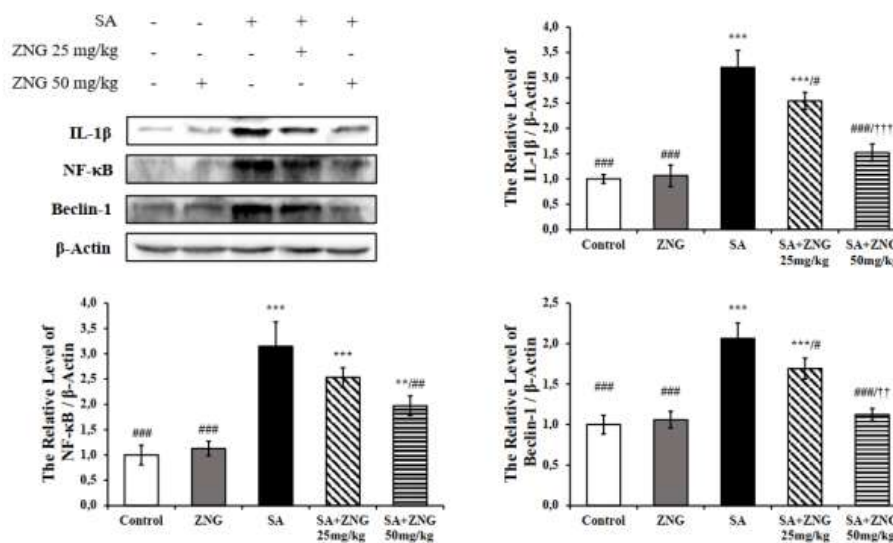


Figure 6. Effects of SA and ZNG administrations on IL-1β, NF-κB, and Beclin-1 protein levels in rat lung tissues
 NF-κB: Nuclear factor kappa-B, IL-1β: interleukin-1 beta. Statistical significance was analyzed using One Way ANOVA (mean ± SD) (Control vs others: *P<0.05, **P<0.01, ***P<0.001, SA 10 mg/kg vs others: #P<0.05, ##P<0.01, ###P<0.001, SA 10 mg/kg+ZNG 25 mg/kg vs SA10 mg/kg+ZNG 50 mg/kg: ☆P<0.05, ☆☆P<0.01, ☆☆☆P<0.001).

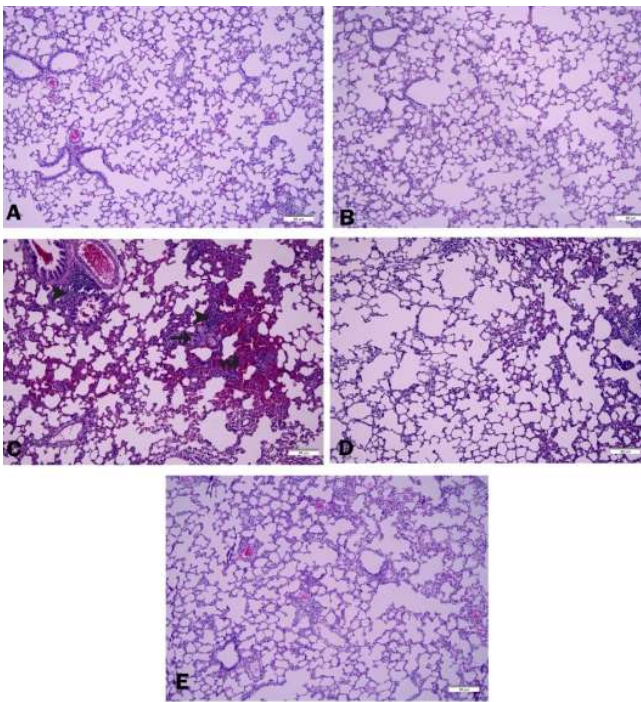


Figure 7. Photomicrographs of histological changes in lung tissue. (Hematoxylin-Eosin: H&E staining, scale bar: 50 μ m)
 A: Control, B: ZNG50 mg/kg; Zingerone group, C: SA10 mg/kg; Sodium arsenite group; arrowhead: infiltration of inflammatory cells, curved arrow: bleeding, arrow: thickening of alveolar wall, D: SA+ZNG 25 mg/kg group; E: SA+ZNG 50 mg/kg group

Discussion

Among environmental pollutants, AR is found all over the world and still affects tens of millions of people worldwide. There are two most dangerous inorganic forms of AR; arsenite and arsenate (23). The maximum acceptable level of AR in drinking water is 0.01 mg/l. However, higher levels have been reported in many drinking waters worldwide, and the more hazardous inorganic forms are more prevalent in drinking water (24). Long and short-term exposure to inorganic forms affects lung tissue (23). An important aspect pointed out in the literature to combat AR-induced body toxicity is the administration of anti-oxidants (25). ZNG is an alkanone with potent anti-oxidant properties that is the active component of ginger (26). As a result, ZNG was chosen as an anti-oxidant in the current study, and the effects of ZNG on OS, inflammation, apoptotic, and autophagy damages in SA-induced rat lung tissue toxicity were investigated by biochemical, molecular, and histopathological methods.

OS occurs when ROS increase and anti-oxidants decrease (27). Lipids, an essential component of the cell membrane, are affected by the increase in ROS. Therefore, ROS increase causes LP. MDA, the end product of multiple fatty acid metabolism (28), is a significant marker of LP and increased OS. Anti-oxidant enzymes CAT, SOD, and GPx reduce OS damage (29). GSH is another protective mechanism against OS by binding ROS products (30). Increased MDA levels in lung tissues of people who drink AR-contaminated water for long periods, together with decreased GSH levels and CAT activity, lead to poor OS and, ultimately, OS-induced DNA strand breakage (31). The most prominent feature of OS in AR toxicity is the increase in LP and the main indicator of this is the increase in MDA (25). When the current study's OS findings were considered together, SA increased OS by

increasing MDA levels and decreasing anti-oxidant enzyme activities in lung tissues. ZNG administration, on the other hand, increased anti-oxidant activity by decreasing SA-induced increased MDA levels and increasing SOD, CAT, and GPx activities. This anti-oxidant activity was stronger, especially at 50 mg/kg dose. Moheemmed reported that ZNG decreased MDA levels by reducing LP and had a protective effect on tissue, which is similar to our findings (13). Kandemir *et al.* reported that ZNG increased anti-oxidant capacity by increasing GSH levels and SOD, CAT, and GPx activities and decreased MDA levels, which is consistent with the data of our study (10). The reason for this effect of ZNG may be a result of its ability to transfer electrons, chelate metals, and scavenge arsenite-induced free radicals by reactivating decreased anti-oxidant enzymes.

In addition to deactivating the anti-oxidant capacity in the body, increased ROS can also impair post-translational protein activities. Moreover, it can affect gene activities by regulating important transcription factors and promoting an inflammatory environment in addition to OS (32). This effect of excessive ROS production is a significant factor in its acting as a signaling molecule to activate NF- κ B. Once NF- κ B is activated, it translocates toward the nucleus to alter the expression of inflammation-related COX-2 and TNF- α genes (33). Studies have reported that COX-2 plays a role in many physiological activities. Different mediators associated with inflammation such as growth factors, lipopolysaccharide, interleukin-1 β , and TNF- α affect COX-2 expression (34). TNF- α is a significant immune response factor that initiates and regulates the cytokine cascade (35). COX-2, TNF- α , and iNOS all play significant roles in inflammation and their activation is mediated by NF- κ B (36). Therefore, inhibiting NF- κ B is therapeutically important in preventing inflammation (37). In the current study, SA caused inflammatory damage in lung tissues by increasing NF- κ B and related proinflammatory cytokines. ZNG administration, on the other hand, reduced SA-induced inflammatory damage by reducing NF- κ B and related proinflammatory cytokines. ZNG could emerge as an effective therapeutic agent in lung toxicity caused by inflammation due to SA exposure. Similar to our study, it was reported that SA administration triggered NF- κ B activation and increased proinflammatory substances such as COX-2 and iNOS, resulting in inflammatory damage (38). On the other hand, consistent with the findings in our study, Akaras *et al.* reported that ZNG administration decreased tissue inflammation by inhibiting NF- κ B activity in SA-induced nephrotoxicity (14). The reason for ZNG's anti-inflammatory effect could be that it tries to reduce the development of inflammation by decreasing ROS production and increasing anti-oxidant gene activation. Because reducing ROS generation prevents NF- κ B translocation to the nucleus and subsequently proinflammatory cytokines will not be stimulated.

MAPK14, also known as p38 α , is known as another key regulator of the inflammatory response (39). The MAPK signaling pathway also activates the inflammation-associated NF- κ B signaling pathway (14, 40). In this study, SA significantly increased MAPK14 activity. In their study with different toxic agents, A study showed that MAPK14 increased lung toxicity, similar to this study (41). The activity of this enzyme was significantly reduced following ZNG administration. It can be stated that SA significantly triggers inflammation by activating both pathways. ZNG

showed an anti-inflammatory effect in this SA-induced lung toxicity with its inhibitory effect on both pathways.

Apoptosis occurs due to DNA or protein damage resulting from excessive ROS production (42, 43). Apoptosis is a process that eliminates cells in the body that are harmful or need to be destroyed. However, if it increases, it causes stress or damage to healthy cells as well (44, 45). Bax is an apoptotic factor and opens membrane pores in mitochondria. Bcl-2 is an antiapoptotic factor that prevents the opening of these pores. Once caspase-3 is active, the irreversible step in the apoptotic process is initiated, which causes proteolytic degradation and death of cells (46). In this study, mRNA transcript levels of Caspase-3 and Bax, which are apoptotic factors, increased with SA exposure in lung tissues, while Bcl-2, which is an antiapoptotic factor, decreased. When ZNG was administered together with SA, the opposite effect was observed and ZNG exhibited antiapoptotic properties. Therefore, ZNG may be an effective agent against apoptosis in SA-induced lung toxicity.

Autophagy is another pathway caused by SA-induced OS (47). Autophagy is a protective mechanism that removes dysfunctional or senescent organelles via lysosomes. In physiological conditions, autophagy plays an active role in cellular homeostasis and occurs at low levels. However, when overstimulated, it brings with it the loss of healthy cells and tissues (48). In this study, Beclin-1 mRNA transcription and protein level, a significant autophagy marker, increased with SA application. This indicates that SA triggers autophagy. ZNG, on the other hand, when combined with SA, showed an antiautophagic effect and decreased Beclin-1 levels. Similar to our study, it was reported that ZNG showed anti autophagic effect by decreasing the Beclin-1 level (49).

Nrf2 is a critical transcription factor co-stimulated by OS. Nrf2 is effective in the regulation of some anti-oxidant genes (50). Once activated, Nrf-2 is transported to the nucleus and regulates the activation of HO-1 and NQO1 (51). HO-1 is one of the target genes of Nrf-2. Increased HO-1 enzyme activity is a potent protective mechanism against ROS-induced OS damage (52, 53). Nrf-2 also initiates the activation of the NQO1 protein. NQO1 protein functions include protecting against natural and exogenous quinones, activating endogenous anti-oxidants, and stabilizing the p53 protein (54). Once the Nrf-2 signaling pathway is active, it can effectively contribute to tissue healing, primarily by preventing OS damage (55). Nrf-2, on the other hand, can directly stop cellular apoptosis by stimulating the expression of BCL-xL (54). For these reasons, Nrf-2 is essential for the relief of lung disorders, and lung tissue pathological processes can be effectively alleviated by activation of Nrf-2 (56). Nrf-2-deficient rats tend to suffer from diseases caused by oxidants and toxic substances, for example, pulmonary damage induced by inhaled AR (51). In this study, Nrf-2, HO-1, and NQO1 levels were decreased by SA exposure in rat lung tissues. Similar to our study, it was reported that Nrf-2, HO-1, and NQO1 parameters decreased with the toxic agent in a different tissue in the body (57). The opposite was observed to increase when ZNG was administered together with SA. This suggests that ZNG causes an increase in anti-oxidant capacity through the Nrf-2 pathway.

Exposure of the human body to SA is usually by ingestion or inhalation. Thus, lung tissue is one of the target tissues of SA exposure and a sensitive one (32). Even acute exposure to different doses of AR causes decreased cell viability and morphological changes (58). The epithelial cell is the main

cell type in the lung and is one of the critical structures affected by lung diseases. In a study, arsenite administration increased collagen fiber deposition in the peri-bronchioles and alveolar region. They reported that AR exposure may trigger both obstructive and restrictive lung diseases (59). Hemorrhages and congestion were remarkable in the tissues administered with SA in our study, especially in the interstitial area. However, it was found that these hemorrhages decreased dose-dependently when ZNG was administered. We found that lung thickening, which increased with SA administration, regressed with ZNG administration. It was remarkable that this thickening was reduced to a minimal level at the dose of 50 mg/kg. In general, it can be stated that SA administration disrupted lung morphology and ZNG administration was used to preserve the morphology.

Conclusion

In summary, ZNG reduced SA-induced toxic damage by reducing OS damage, inflammation damage, apoptotic and autophagic cell death, and activating anti-oxidant defense systems in rat lung tissues. The present study supports the hypothesis that ZNG may have a protective effect in SA-induced damage to rat lung tissues.

Acknowledgment

This study was financed by the authors' funds.

Authors' Contributions

All authors contributed to the concept and design of this study, also to material preparation, data collection, and analysis. All authors have read and approved the article written by H Ş.

Ethical Approval

Ethical approval was obtained by Atatürk University Animal Experiments Local Ethics Committee (No: 2022/11-238, Date: 27.10.2022).

Consent to Participate

All authors have given their explicit consent for the publication of the manuscript. Hasan Şimşek has the consent of all authors for contact by anyone for further clarification and information about the research if necessary.

Conflicts of Interest

The authors have no conflicts of interest.

References

1. Caglayan C, Taslimi P, Türk C, Gulcin İ, Kandemir FM, Demir Y, Beydemir Ş. Inhibition effects of some pesticides and heavy metals on carbonic anhydrase enzyme activity purified from horse mackerel (*Trachurus trachurus*) gill tissues. *Environ Sci Pollut Res Int* 2020;27:10607-10616.
2. Adeyi OE, Babayemi DO, Ajayi BO, Adeyi AO, Ayodeji AH, Oguntayo AO, *et al.* Co-administration of sodium selenite and sodium arsenite exacerbates hepatic, renal, pulmonary and splenic inflammation in rats. *Sci Afr* 2021;11:e00708.
3. Turk E, Kandemir FM, Yildirim S, Caglayan C, Kucukler S, Kuzu M. Protective effect of hesperidin on sodium arsenite-induced nephrotoxicity and hepatotoxicity in rats. *Biol Trace Elem Res* 2019;189:95-108.
4. Sun M, Tan J, Wang M, Wen W, He Y. Inorganic arsenic-mediated upregulation of AS3MT promotes proliferation of

- nonsmall cell lung cancer cells by regulating cell cycle genes. *Environ Toxicol* 2021;36:204-212.
5. Kuzu M, Kandemir FM, Yildirim S, Çağlayan C, Küçükler S. Attenuation of sodium arsenite-induced cardiotoxicity and neurotoxicity with the anti-oxidant, anti-inflammatory, and antiapoptotic effects of hesperidin. *Environ Sci Pollut Res Int* 2021;28:10818-10831.
 6. Hosseinzadeh A, Houshmand G, Goudarzi M, Sezavar SH, Mehrzadi S, Mansouri E, et al. Ameliorative effect of gallic acid on sodium arsenite-induced spleno-cardio- and hemato-toxicity in rats. *Life Sci* 2019;217:91-100.
 7. Akanda MR, Tae HJ, Kim IS, Ahn D, Tian W, Islam A, et al. Hepatoprotective role of hydrangea macrophylla against sodium arsenite-induced mitochondrial-dependent oxidative stress via the inhibition of MAPK/Caspase-3 pathways. *Int J Mol Sci* 2017;18:1-15.
 8. Momeni HR, Eskandari N. Effect of curcumin on kidney histopathological changes, lipid peroxidation and total antioxidant capacity of serum in sodium arsenite-treated mice. *Exp Toxicol Pathol* 2017;69:93-97.
 9. Wang YC, Chaung RH, Tung LC. Comparison of the cytotoxicity induced by different exposure to sodium arsenite in two fish cell lines. *Aquat Toxicol* 2004;69:67-79.
 10. Kandemir FM, Yildirim S, Caglayan C, Kucukler S, Eser G. Protective effects of zingerone on cisplatin-induced nephrotoxicity in female rats. *Environ Sci Pollut Res Int* 2019;26:22562-22574.
 11. Gungor H, Ekici M, Onder Karayigit M, Turgut NH, Kara H, Arslanbas E. Zingerone ameliorates oxidative stress and inflammation in bleomycin-induced pulmonary fibrosis: modulation of the expression of TGF- β 1 and iNOS. *Naunyn Schmiedebergs Arch Pharmacol* 2020;393:1659-1670.
 12. Kucukler S, Darendelioğlu E, Caglayan C, Ayna A, Yildirim S, Kandemir FM. Zingerone attenuates vancomycin-induced hepatotoxicity in rats through regulation of oxidative stress, inflammation and apoptosis. *Life Sci* 2020;259:118382.
 13. Mohammed HM. Zingerone ameliorates non-alcoholic fatty liver disease in rats by activating AMPK. *J Food Biochem* 2022;46:e14149.
 14. Akaras N, Gur C, Kucukler S, Kandemir FM. Zingerone reduces sodium arsenite-induced nephrotoxicity by regulating oxidative stress, inflammation, apoptosis and histopathological changes. *Chem Biol Interact* 2023 Apr 1;374:110410.
 15. Placer ZA, Cushman LL, Johnson BC. Estimation of product of lipid peroxidation (malonyl dialdehyde) in biochemical systems. *Anal Biochem* 1966; 16: 359-364.
 16. Aebi H. Catalase *in vitro*. *Methods Enzymol* 1984; 105: 121-126.
 17. Sun Y, Oberley LW, Li Y. A simple method for clinical assay of superoxide dismutase. *Clin Chem* 1988; 34: 497-500.
 18. Lawrence RA, Burk RF. Glutathione peroxidase activity in selenium-deficient rat liver. 1976. *Biochem Biophys Res Commun* 2012; 425: 503-509.
 19. Sedlak J, Lindsay RH. Estimation of total, protein-bound, and nonprotein sulfhydryl groups in tissue with Ellman's reagent. *Anal Biochem* 1968; 25: 192-205.
 20. Lowry OH, Rosebrough NJ, Farr AL, Randall RJ. Protein measurement with the Folin phenol reagent. *J Biol Chem* 1951;193:265-275.
 21. Livak KJ, Schmittgen TD. Analysis of relative gene expression data using real-time quantitative PCR and the 2- $\Delta\Delta$ CT method. *Methods* 2001;25:402-408.
 22. Ileriturk M, Kandemir O, Kandemir FM. Evaluation of protective effects of quercetin against cypermethrin-induced lung toxicity in rats via oxidative stress, inflammation, apoptosis, autophagy, and endoplasmic reticulum stress pathway. *Environ Toxicol* 2022;37:2639-2650.
 23. Al-Brakati AY, Kassab RB, Lokman MS, Elmahallawy EK, Amin HK, Abdel Moneim AE. Role of thymoquinone and ebselen in the prevention of sodium arsenite-induced nephrotoxicity in female rats. *Hum Exp Toxicol* 2019;38:482-493.
 24. Souza ACF, Bastos DSS, Couto-Santos F, Guimarães-Ervilha LO, Araujo LS, Souza PHCA, et al. Long-term reproductive effects in male rats prenatally exposed to sodium arsenite. *Environ Toxicol* 2023 May;38:1162-1173.
 25. Oyibo A, Gbadegesin MA, Odunola OA. Ethanol extract of *Vitellaria paradoxa* (Gaertn, F) leaves protects against sodium arsenite - induced toxicity in male Wistar rats. *Toxicol Rep* 2021;8:774-784.
 26. Xie X, Sun S, Zhong W, Soromou LW, Zhou X, Wei M, et al. Zingerone attenuates lipopolysaccharide-induced acute lung injury in mice. *Int Immunopharmacol* 2014; 19:103-109.
 27. El-belbasy HI, Hussein MA, Alghitany MEM. Potential effects of cranberry extract against lead acetate-induced hepatorenal toxicity in rats. *Adv Anim Vet Sci* 2021;9:1669-1683
 28. Aksu EH, Kandemir FM, Özkaraca M, Ömür AD, Küçükler S, Çomaklı S. Rutin ameliorates cisplatin-induced reproductive damage via suppression of oxidative stress and apoptosis in adult male rats. *Andrologia* 2017; 49: e12593.
 29. Çelik H, Kucukler S, Çomaklı S, Özdemir S, Caglayan C, Yardım A, et al. Morin attenuates ifosfamide-induced neurotoxicity in rats via suppression of oxidative stress, neuroinflammation and neuronal apoptosis. *Neurotoxicology* 2020;76:126-137.
 30. Gur C, Kandemir O, Kandemir FM. Investigation of the effects of hesperidin administration on abamectin-induced testicular toxicity in rats through oxidative stress, endoplasmic reticulum stress, inflammation, apoptosis, autophagy, and JAK2/STAT3 pathways. *Environ Toxicol* 2022;37:401-412.
 31. Yamanaka K, Hasegawa A, Sawamura R, Okada S. Dimethylated arsenics induce DNA strand breaks in lung via the production of active oxygen in mice. *Biochem Biophys Res Commun* 1989;165:43-50.
 32. Mahalanobish S, Saha S, Dutta S, Sil PC. Mangiferin alleviates arsenic induced oxidative lung injury via upregulation of the Nrf2-HO1 axis. *Food Chem Toxicol* 2019;126:41-55.
 33. Rana MN, Tangpong J, Rahman MA. Xanthon protects lead-induced chronic kidney disease (CKD) via activating Nrf-2 and modulating NF- κ B, MAPK pathway. *Biochem Biophys Rep* 2019;21:100718.
 34. İkinci Akdemir FN, Yildirim S, Kandemir FM, Tanyeli A, Küçükler S, Bahaeddin Dortbudak M. Protective effects of gallic acid on doxorubicin-induced cardiotoxicity; an experimental study. *Arch Physiol Biochem* 2021;127:258-265.
 35. Kandemir FM, Caglayan C, Aksu EH, Yildirim S, Kucukler S, Gur C, et al. Protective effect of rutin on mercuric chloride-induced reproductive damage in male rats. *Andrologia* 2020;52:e13524.
 36. Ileriturk M, Benzer F, Aksu EH, Yildirim S, Kandemir FM, Dogan T, et al. Chrysin protects against testicular toxicity caused by lead acetate in rats with its anti-oxidant, anti-inflammatory, and anti-apoptotic properties. *J Food Biochem* 2021;45:e13593.
 37. Kucukler S, Benzer F, Yildirim S, Gur C, Kandemir FM, Bengu AS, et al. Protective effects of chrysin against oxidative stress and inflammation induced by lead acetate in rat kidneys: a biochemical and histopathological approach. *Biol Trace Elem Res* 2021;199:1501-1514.
 38. Fouad AA, Albuali WH, Al-Mulhim AS, Jresat I. Protective effect of telmisartan treatment against arsenic-induced testicular toxicity in rats. *Z Naturforsch C J Biosci* 2015;70:175-181.
 39. Caglayan C, Kandemir FM, Yildirim S, Kucukler S, Eser G. Rutin protects mercuric chloride-induced nephrotoxicity via targeting of aquaporin 1 level, oxidative stress, apoptosis and inflammation in rats. *J Trace Elem Med Biol* 2019;54:69-78.
 40. Yang X, Gao X, Du B, Zhao F, Feng X, Zhang H, et al. *Ilex asprella* aqueous extracts exert *in vivo* anti-inflammatory effects by regulating the NF- κ B, JAK2/STAT3, and MAPK signaling pathways. *J Ethnopharmacol* 2018;225:234-243.
 41. Abdel-Latif GA, Elwahab AHA, Hasan RA, ElMongy NF,

- Ramzy MM, Louka ML, et al. A novel protective role of sacubitril/valsartan in cyclophosphamide induced lung injury in rats: Impact of miRNA-150-3p on NF- κ B/MAPK signaling trajectories. *Sci Rep* 2020;10:13045.
42. Caglayan C, Kandemir FM, Darendelioglu E, Yildirim S, Kucukler S, Dortbudak MB. Rutin ameliorates mercuric chloride-induced hepatotoxicity in rats via interfering with oxidative stress, inflammation and apoptosis. *J Trace Elem Med Biol* 2019;56:60-68.
43. Abdelhamid FM, Mahgoub HA, Ateya AI. Ameliorative effect of curcumin against lead acetate-induced hemato-biochemical alterations, hepatotoxicity, and testicular oxidative damage in rats. *Environ Sci Pollut Res Int* 2020;27:10950-10965.
44. Akcilar R, Akcilar A, Koçak C, Koçak FE, Bayat Z, Şimşek H, et al. Effects of Ukrain on intestinal apoptosis caused by ischemia-reperfusion injury in rats. *Int J Clin Exp Med* 2015;8:22158-22166.
45. Ileriturk M, Kandemir O, Akaras N, Simsek H, Genc A, Kandemir FM. Hesperidin has a protective effect on paclitaxel-induced testicular toxicity through regulating oxidative stress, apoptosis, inflammation and endoplasmic reticulum stress. *Reprod Toxicol* 2023;118:108369.
46. Kuzu M, Kandemir FM, Yildirim S, Kucukler S, Caglayan C, Turk E. Morin attenuates doxorubicin-induced heart and brain damage by reducing oxidative stress, inflammation and apoptosis. *Biomed Pharmacother* 2018;106:443-453.
47. Huang YC, Hung WC, Chen WT, Yu HS, Chai CY. Sodium arsenite-induced DAPK promoter hypermethylation and autophagy via ERK1/2 phosphorylation in human uroepithelial cells. *Chem Biol Interact* 2009;181:254-262.
48. Aksu EH, Kandemir FM, Küçükler S. The effects of hesperidin on colistin-induced reproductive damage, autophagy, and apoptosis by reducing oxidative stress. *Andrologia* 2021;53:e13900.
49. Shahidi M, Moradi A, Dayati P. Zingerone attenuates zearalenone-induced steroidogenesis impairment and apoptosis in TM3 Leydig cell line. *Toxicol* 2022;211:50-60.
50. Xiong L, Huang J, Gao Y, Gao Y, Wu C, He S, et al. Sodium arsenite induces spatial learning and memory impairment associated with oxidative stress and activates the Nrf2/PPAR γ pathway against oxidative injury in mice hippocampus. *Toxicol Res (Camb)* 2021;10:277-283.
51. Li GH, Li AL, Chen XM, Zhang LY, Wang T, Wang XN, et al. Naturally-derived diterpenoid sphaeropsidin C as an activator of Nrf2/ARE pathway and its potential capability of relieving intracellular oxidative stress in human lung epithelial cells. *Biomed Pharmacother* 2020;121:109669.
52. Hung SY, Liou HC, Kang KH, Wu RM, Wen CC, Fu WM. Overexpression of heme oxygenase-1 protects dopaminergic neurons against 1-methyl-4-phenylpyridinium-induced neurotoxicity. *Mol Pharmacol* 2008;74:1564-1575.
53. Habtemariam S. The Nrf2/HO-1 axis as targets for flavanones: Neuroprotection by pinocembrin, naringenin, and eriodictyol. *Oxid Med Cell Longev* 2019;2019:4724920.
54. Kong Q, Deng H, Li C, Wang X, Shimoda Y, Tao S, et al. Sustained high expression of NRF2 and its target genes induces dysregulation of cellular proliferation and apoptosis is associated with arsenite-induced malignant transformation of human bronchial epithelial cells. *Sci Total Environ* 2021;756:143840.
55. Jaramillo MC, Zhang DD. The emerging role of the Nrf2-Keap1 signaling pathway in cancer. *Genes Dev* 2013;27:2179-2191.
56. Wang T, Sun XY, Li AL, Zhou MX, Han Y, Zhang JZ, et al. Botryspin D attenuates arsenic-induced oxidative stress in human lung epithelial cells via activating Nrf2/ARE signaling pathways. *Biochem Biophys Res Commun* 2019;518:526-532.
57. Şimşek H, Akaras N, Gür C, Küçükler S, Kandemir FM. Beneficial effects of chrysin on cadmium-induced nephrotoxicity in rats: Modulating the levels of Nrf2/HO-1, RAGE/NLRP3, and Caspase-3/Bax/Bcl-2 signaling pathways. *Gene* 2023;875:147502.
58. Kim C, States JC, Ceresa BP. Chronic and acute arsenic exposure enhance EGFR expression via distinct molecular mechanisms. *Toxicol In Vitro* 2020;67:104925.
59. Chiou HY, Wang CW, Chen SC, Wu DW, Lin HH, Liao WT, et al. Arsenic exposure and pulmonary fibrosis-evidences from a longitudinal cohort study and experimental models. *SSRN* 2022; 1-26.